JCTC Journal of Chemical Theory and Computation

ARTICLE

pubs.acs.org/JCTC

Using Theory to Reconcile Experiment: The Structural and Thermodynamic Basis of Ligand Recognition by Phenylethanolamine *N*-Methyltransferase (PNMT)

Pramod C. Nair,[†] Alpeshkumar K. Malde,[†] and Alan E. Mark*[,†,‡]

[†]School of Chemistry and Molecular Biosciences (SCMB) and [‡]Institute for Molecular Bioscience (IMB), The University of Queensland (UQ), St. Lucia Campus, Brisbane, QLD 4072 Australia

ABSTRACT: A fundamental challenge in computational drug design is the availability of reliable and validated experimental binding and structural data against which theoretical calculations can be compared. In this work a combination of molecular dynamics (MD) simulations and free energy calculations has been used to analyze the structural and thermodynamic basis of ligand recognition by phenylethanolamine *N*-methyltransferase (PNMT) in an attempt to resolve uncertainties in the available binding and structural data. PNMT catalyzes the conversion of norepinephrine into epinephrine (adrenaline), and inhibitors of PNMT are of potential therapeutic importance in Alzheimer's and Parkinson's disease. Excellent agreement between the calculated and recently revised relative binding free energies to human PNMT was obtained with the average deviation between the calculated and the experimentally determined values being only 0.8 kJ/mol. In this case, the variation in the experimental data over time is much greater than the uncertainties in the theoretical estimates. The calculations have also enabled the refinement of structure−activity relationships in this system, to understand the basis of enantiomeric selectivity of substitution at position three of tetrahydroisoquinoline and to identify the role of specific structural waters. Finally, the calculations suggest that the preferred binding mode of *trans*-(1*S*,2*S*)-2-amino-1-tetralol is similar to that of its epimer *cis*-(1*R*,2*S*)-2-amino-1-tetralol and that the ligand does not adopt the novel binding mode proposed in the pdb entry 2AN5. The work demonstrates how MD simulations and free energy calculations can be used to resolve uncertainties in experimental binding affinities, binding modes, and other aspects related to X-ray refinement and computational drug design.

INTRODUCTION

The primary challenge in rational drug design is to understand how a protein recognizes a specific ligand. X-ray structures of protein−ligand complexes can provide detailed information regarding the location of the ligand within the complex and information on specific ligand-protein interactions. They do not, however, provide information on how these interactions may contribute to the net binding free energy. Thus, the question of why a specific ligand binds better than another is frequently open to speculation.[1−3] An additional difficulty is that the binding mode (the position, the orientation, and the conformation) of small ligands can be uncertain in medium-(0.2−0.3 nm) to low-(>0.3 nm) resolution structures where alternative binding modes cannot be distinguished based solely on the electron density.[4,5] In such cases the combined use of molecular dynamics (MD) simulations and free energy calculations (FE) has proved to be a powerful approach to identify the thermodynamically stable binding mode. For example, Malde and Mark[5] recently discussed a number of examples where the stereochemistry, conformation, and orientation and the protonation and tautomeric states of specific ligand structures were ambiguous and where the published structures were possibly inappropriate. A case in point was the binding of noradrenochrome and tetrahydroisoquinoline-7-sulphonamide to phenyl ethanolamine *N*-methyltransferase (PNMT). In particular, the novel binding mode proposed in the case of noradrenochrome and the proposed orientation of the sulphonamide group in the ligand tetrahydroisoquinoline-7-sulphonamide were unstable, suggesting that the crystallographic models represented high-energy states.

PNMT catalyzes the formation of epinephrine (adrenaline) from norepinephrine.[6] In the central nervous system (CNS) epinephrine is linked to the control of blood pressure and respiration as well as the secretion of pituitary hormones.[7,8] CNS specific PNMT inhibitors are of potential therapeutic importance as the progression of diseases, such as Alzheimer's and Parkinson's diseases, is associated with increased levels of epinephrine in the CNS.[9−12] Several classes of PNMT inhibitors have been identified. These include derivatives of phenylethylamine and α-methylphenethylamine (amphetamine) as well as sulfhydryl-binding agents and benzamidine-based compounds.[9,10] While many of these compounds are potent inhibitors of PNMT in vitro, the design of inhibitors that are active in vivo and in particular within the CNS remains a significant challenge. For example, phenylethylamine- and benzamidine-based PMNT inhibitors are of little use clinically as they show cross reactivity with the α-adrenergic receptor.[13] Tetrahydroisoquinoline (THIQ) (Figure 1, molecule **1**) derivatives are also potent inhibitors of PNMT in vitro and exhibit good selectivity.[14,15] It has also been claimed that derivatives of THIQ should be active within the CNS.[14,16] THIQ is a structural analog of norepinephrine, the main substrate of PMNT. Based on structure−activity relationships (SAR), it has been reported that the combination of an electron-withdrawing substituent at position 7 and an alkyl substituent at position 3 on the THIQ scaffold (see Figure 1) leads to enhanced PNMT inhibition with good selectivity over the α-adrenergic receptor.[17−19] A number of X-ray crystal structures of PNMT:THIQ complexes have been

Received: December 16, 2010
Published: March 30, 2011

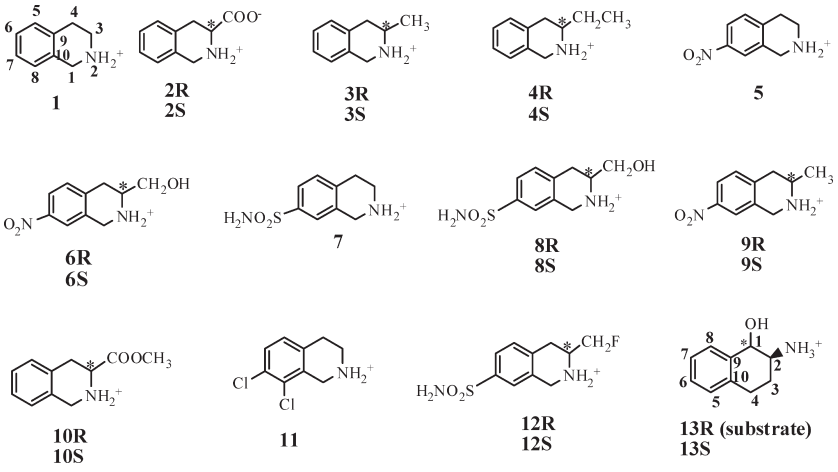

Figure 1. Three-, seven-, and eight-substituted tetrahydroisoquinoline (THIQ) derivatives and 2-amino-1-tetralol used in the study. The numbering scheme for THIQ and 2-amino-1-tetralol is given for ligands **1** and **13**, respectively; * indicates the chiral center.

reported. In these structures the bulkier substituents at position 7 of the THIQ ring were found to bind within a pocket which is not evident in the ligand-free protein, suggesting that the protein has a high degree of conformational plasticity complicating structure-based ligand design.[20,21] Detailed analysis of this system is further complicated by the fact that there is uncertainty regarding the experimental binding data.[21−24] This is illustrated in Table 1, which lists experimental binding data for the PNMT inhibitors shown in Figure 1. As can be seen, differences of between 10- and a 1000-fold in the value of K_i, which corresponds to an uncertainty of between 5 and 11 kJ/mol in the free energy of binding, have been reported by the same authors using different assay conditions.[23] In addition, binding data is only available for racemic mixtures in several cases or only for one of the potential isomers in others.

In the present study a combination of MD simulations and FE calculations have been used in order to understand in detail the structural and thermodynamic basis of ligand recognition by PNMT. A series of THIQ derivatives with substitutions at positions three, seven, and eight that shows a wide range of binding free energies (−48 to > −15 kJ/mol) and the potential enantiomeric selectivity have been examined.[19,21,23−27] Excellent agreement between the calculated and the recent experimental values for the FE of binding of these THIQ derivatives to human PNMT was obtained with the variation in the experimental data over time being much greater than the uncertainties in the theoretical estimates. In addition, alternative binding modes of *trans*-(1*S*,2*S*)-2-amino-1-tetralol (Figure 1, **13S**) to human PNMT have been considered and the role specific water molecules play in stabilizing the binding of *cis*-(1*R*,2*S*)-2-amino-1-tetralol (Figure 1, **13R**) to PNMT was examined.

METHODS

MD Simulations. All MD simulations were performed using the GROMOS96 simulation package in conjunction with the GROMOS 53A6 force field.[28,29] The initial structure of human PNMT complexed with the cofactor *S*-adenosyl-L-homocysteine (SAH) and 1,2,3,4-tetrahydro-isoquinoline-7-sulphonamide (inhibitor **7**) taken from the pdb entry 1HNN was used for all studies involving THIQ derivatives. The initial structures for the studies involving the binding of **13R** and **13S** were taken from pdb entries 2AN3 and 2AN5, respectively. The topologies of the ligands (Figure 1) were generated using the 'Automated Topology Builder' (ATB, http://compbio.biosci.uq.edu.au/atb/), version 2009-06-10.[30] Missing parameters were manually assigned where possible based on comparable groups within the GROMOS force field.[29] The parameters used for the $-NO_2$ and $-SO_2NH_2$ groups are shown in Tables 2a and 2b. Simulations of the ligands free in solution were performed by placing the ligand in a periodic rectangular box containing 975 simple point charge (SPC) water molecules.[31] For the systems in which the ligand was bound to the protein, the configuration of the solvent was relaxed by performing a steepest descent minimization in which the protein and ligand atoms were positionally restrained to their initial positions using a harmonic interaction potential with a force constant of 2×10^3 kJ/mol/nm^2. The system was then further equilibrated by performing a 200 ps simulation, with the heavy atoms of the protein positionally restrained, before a series of unrestrained MD simulations were commenced. All the simulations were performed at constant temperature (298 K) and pressure (1 atm). This was achieved using a Berendsen thermostat[32] with a coupling time of 0.1 ps and a Berendsen barostat with a coupling time of 0.5 ps. The isothermal compressibility was set to 4.575×10^{-4} kJ/mol/nm^3. Nonbonded interactions were calculated using a twin-range cutoff. Interactions within the short-range cutoff of 0.8 nm were updated every time step. Interactions within the longer-range cutoff of 1.4 nm were updated every 5 time steps together with the pairlist. To correct for the truncation of electrostatic interactions beyond the 1.4 nm long-range cutoff, a reaction field correction was applied using an effective dielectric (ε) of 54.[28] The equations of motion were integrated using the leapfrog scheme with a 2 fs time step. Initial velocities at a given temperature were taken from a Maxwell−Boltzmann distribution. The lengths of all bonds were constrained to ideal values using the SHAKE algorithm with a geometric tolerance of 0.0001.[33]

System Setup. The initial structure of the different protein: ligand complexes were derived from the crystal structure of PNMT complexed with 1,2,3,4-tetrahydroisoquinoline-7- sulphonamide (inhibitor **7**) and the cofactor *S*-adenosyl-L-homocysteine, pdb code 1HNN.[34] The GROMOS force field treats aliphatic hydrogen atoms as united atoms together with the carbon atom to which they are attached. The coordinates of polar hydrogen atoms (bound to nitrogen, oxygen, or sulfur atoms)

Table 1. Experimental (Human and/or Bovine) and Calculated (Human) Relative Gibbs Free Energies of Binding (Calculated Relative to Inhibitor 5) with PNMT[a]

	inhibitor	K_i (μM)	ref	ΔG_{expt} (kJ/mol)	relative $\Delta\Delta G_{expt}$ (kJ/mol)	relative $\Delta\Delta G_{calcd}$ (kJ/mol) [d]	$\Delta\Delta G_{expt} - \Delta\Delta G_{calcd}$ (kJ/mol)
1	**1**	15.0 ± 1	22	−27.8 ± 0.2	13.1 ± 0.6	9.7 ± 1.8	3.4
2		***5.8 ± 0.5***	24	***−30.1 ± 0.2***	***10.8 ± 0.6***	***9.7 ± 1.8***	***1.1***
3	**1**[b]	10.0 ± 0.9	19, 25	−28.8 ± 0.2	12.1 ± 0.6	9.7 ± 1.8	2.4
4	**2**[b,c]	>2000	25	> −15.5	>25.4	–	–
5	**2R**	–	–	–	–	66.9 ± 2.5	–
6	**2S**	–	–	–	–	99.5 ± 1.6	–
7	**3R**[b]	38.0 ± 2	19	−25.4 ± 0.1	15.5 ± 0.5	14.0 ± 2.4	1.5
8	**3S**[b]	1.0 ± 0.1	19	−34.5 ± 0.2	6.4 ± 0.6	4.8 ± 2.0	1.6
9	**4**[b,c]	24.0 ± 1	19, 25	−26.6 ± 0.1	14.3 ± 0.5	–	–
10	**4R**	–	–	–	–	8.6 ± 2.6	–
11	**4S**	–	–	–	–	4.2 ± 2.1	–
12	**5**	0.078 ± 0.014	21	−40.9 ± 0.4	0.0	0.0	0.0
13	**6R**	***0.017 ± 0.01***	21	***−44.7 ± 0.1***	***−3.8 ± 0.5***	***−4.6 ± 2.2***	***0.8***
14	**6R**[b]	0.24 ± 0.04	19	−38.1 ± 0.4	2.8 ± 0.8	−4.6 ± 2.2	7.4
15	**6S**[b]	0.9 ± 0.03	19	−34.8 ± 0.1	6.1 ± 0.5	3.1 ± 2.1	3.0
16	**7**	0.58 ± 0.04	22	−35.9 ± 0.2	5.0 ± 0.6	−1.8 ± 2.5	6.8
17		0.28 ± 0.02	23, 27	−37.7 ± 0.1	3.2 ± 0.5	−1.8 ± 2.5	5.0
18		***0.12 ± 0.02***	21, 26	***−39.8 ± 0.3***	***1.1 ± 0.7***	***−1.8 ± 2.5***	***2.9***
19	**7**[b]	0.56 ± 0.04	22	−35.8 ± 0.1	4.9 ± 0.5	−1.8 ± 2.5	6.7
20	**8R**	2.1 ± 0.1	22	−32.7 ± 0.1	8.2 ± 0.5	−0.8 ± 2.3	9.0
21		***0.052 ± 0.004***	24	***−41.9 ± 0.1***	***−1.0 ± 0.5***	***−0.8 ± 2.3***	***−0.2***
22	**8R**[b]	0.34 ± 0.06	22	−37.2 ± 0.3	3.7 ± 0.7	−0.8 ± 2.3	4.5
23	**8S**	–	–	–	–	1.0 ± 2.9	–
24	**9R**[b]	1.3 ± 0.1	19	−33.9 ± 0.2	7.0 ± 0.6	10.2 ± 2.1	−3.2
25	**9S**[b]	0.25 ± 0.02	19	−38.0 ± 0.2	2.9 ± 0.6	−2.1 ± 1.3	5.0
26	**10**[b,c]	69.5 ± 6	19, 25	−24.0 ± 0.3	16.9 ± 0.7	–	–
27	**10R**	–	–	–	–	12.7 ± 2.8	–
28	**10S**	–	–	–	–	22.3 ± 2.8	–
29	**11**	0.3 ± 0.04	22	−37.5 ± 0.2	3.4 ± 0.6	−8.3 ± 2.2	11.7
30		***0.0031 ± 0.0006***	16, 23	***−48.9 ± 0.3***	***−8.0 ± 0.7***	***−8.3 ± 2.2***	***0.3***
31	**11**[b]	0.22 ± 0.05	22	−38.3 ± 0.5	2.6 ± 0.9	−8.3 ± 2.2	10.9
32	**12R**[b]	0.15 ± 0.01	16	−39.3 ± 0.2	1.6 ± 0.6	−1.7 ± 2.5	3.3
33	**12S**	–	–	–	–	9.3 ± 2.3	–

[a] The values in the bold italics correspond to the most recent experimental data for binding to human PNMT at the time of publication. [b] Data for binding to bovine PNMT. [c] Racemic mixture. [d] The standard error for the relative free energy involving two legs were calculated by formula $[(s_1)^2 + (s_2)^2]^{1/2}$, where $s_1$and s_2 are standard errors of two different legs.

and aromatic hydrogen atoms were generated based on ideal geometries. In the chain A of pdb 1HNN, the first 21 N-terminal residues were not resolved. In addition atoms were missing in seven other residues. The missing N-terminal residues were not included in the model as they lie far from the active site. The coordinates for the missing atoms in residues Arg33, Lys136, Arg145, Gln163, Glu241, Arg245, and Leu282 were generated as follows: All atoms in the protein for which the coordinates were available were positionally restrained using a harmonic restraining potential and a force constant of 2×10^3 kJ/mol/nm^2. The coordinates for the other atoms were arbitrarily set to zero. A series of minimizations were then performed in which the bond length, the bond angle, the dihedral, the improper dihedral, and finally the nonbonded terms for the missing atoms were added progressively. After that the restraints were removed, and the whole protein was minimized. The charges of the ionizable groups were chosen to correspond to a pH of 7, resulting in a net charge of −2e. No counterions were added. The histidine residues were assigned appropriate tautomeric configurations based on the local environment of these residues. The protein was placed at the center of a periodic truncated octahedral box, which was filled with 7239 SPC water molecules. In this procedure, the minimum distance between water oxygen atoms and nonhydrogen protein atoms was 0.23 nm, and the minimum distance between the protein and the wall of the box was 0.9 nm.

Free Energy Calculations. The change in Gibbs FE (ΔG), associated with different mutations of the ligand in water and in the protein was determined using the coupling parameter approach in conjunction with the thermodynamic integration eq 1:

$$\Delta G_{0 \to 1} = \int_{\lambda=0}^{\lambda=1} \left\langle \frac{\partial H(\lambda)}{\partial \lambda} \right\rangle_{\lambda} d\lambda \qquad (1)$$

Table 2a. Bonded and Nonbonded Parameters for the Functional Group $-NO_2$

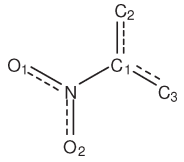

atom[a]	atom type	[C6(i,i)]$^{1/2}$ [(kJ/mol nm^6)$^{1/2}$][b]	[C12(i,i)]$^{1/2}$ [10^{-3} (kJ/mol nm^{12})$^{1/2}$][b]	partial atomic charge (e)
N	7	0.04936	1.523, 2.250	0.700
O1	1	0.04756	1.000, 1.130	0.350
O2	1	0.04756	1.000, 1.130	0.350
C1	12	0.04838	2.222	0.000

bond	bond type	bond length b_0 (nm)	force constant K_b (10^6kJ/mol/nm^4)
C1−N	21	0.147	8.71
N−O1, N−O2	5	0.123	16.6

angle	angle type	bond angle θ_0 (°)	force constant K_θ (kJ/mol)
C1−N−O1, C1−N−O2	22	117	635
O1−N−O2	36	126	575

dihedral	dihedral type	phase shift cos(δ)	force constant K_φ (kJ/mol)	multiplicity m
C2−C1−N−O1	14	−1	33.5	2

improper dihedral angle	improper dihedral type	improper dihedral angle ξ_0 (deg)	force constant K_ξ (kJ/mol/deg^2)
N−O1−O2−C1	1	0.0	0.0510

[a] The carbon C2 and C3 have standard parameters for aromatic carbons in the GROMOS 53A6 parameter set. [b] Lennard-Jones parameters C6(i,j) and C12(i,j) were obtained using the following combination rules: $C_6(i,j) = [C_6(i,i)^{1/2}\ C_6(j,j)^{1/2}]$ and $C_{12}(i,j) = [C_{12}(i,i)^{1/2}\ C_{12}(j,j)^{1/2}]$. The atom, bond, angle, and dihedral types are from the GROMOS 53A6 parameter set.[29]

Table 2b. Bonded and Nonbonded Parameters for the Functional Group $-SO_2NH_2$

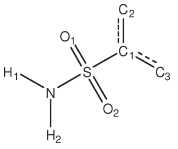

atom[a]	atom type	[C6(i,i)]$^{1/2}$ [(kJ/mol nm^6)$^{1/2}$][b]	[C12(i,i)]$^{1/2}$ [10^{-3} (kJ/mol nm^{12})$^{1/2}$][b]	partial atomic charge (e)
S	42	0.10277	4.6366	1.157
O1	44	0.047652	0.86686, 1.1250	−0.550
O2	44	0.047652	0.86686, 1.1250	−0.561
N	6	0.04936	1.523, 1.943	−0.832
H1	21	0.0	0.0	0.393
H2	21	0.0	0.0	0.393
C1	12	0.04838	2.222	0.000

bond	bond type	bond length b_0 (nm)	force constant K_b (10^6 kJ/mol/nm^4)
C1−S	31	0.178	5.94
S−O	25	0.150	8.37
S−N	41	0.153	8.04

angle	angle type	bond angle θ_0 (°)	force constant K_θ (kJ/mol)
C1−S−N, C1−S−O1, O1−S−O2, O1−S−N	13	109.5	520

dihedral	dihedral type	phase shift cos(δ)	force constant K_φ (kJ/mol)	multiplicity m
C2−C1−S−N	43[c]	+1	0.75	2
C1−S−N−H1	40	+1	1.0	6

improper dihedral angle	improper dihedral type	improper dihedral angle ξ_0 (°)	force constant K_ξ (kJ/mol/deg^2)
N−H1−H2-S	1	0.0	0.0510

[a] The carbon C2 and C3 have standard parameters for aromatic carbons in the GROMOS 53A6 parameter set. [b] Lennard-Jones parameters C6(i,j) and C12(i,j) were obtained using the following combination rules: $C_6(i,j) = [C_6(i,i)^{1/2}\ C_6(j,j)^{1/2}]$ and $C_{12}(i,j) = [C_{12}(i,i)^{1/2}\ C_{12}(j,j)^{1/2}]$. The atom, bond, angle, and dihedral types are from the GROMOS 53A6 parameter set.[29] [c] Nonstandard dihedral type derived by fitting the molecular mechanics (MM) dihedral profile to the one obtained from quantum mechanical (QM) calculations (data not shown).

where $\lambda = 0$ corresponded to the initial state of the system, and $\lambda = 1$ corresponded to the final state of the system. H is the Hamiltonian of the system, and the brackets $<...>_\lambda$ correspond to an average over an equilibrium ensemble at λ. The relative FE of binding $\Delta\Delta G$ was determined from the difference in the change in FE of performing the same mutation free in solution and bound to the protein. Equation 1 was integrated by performing separate simulations at a series of 15 (0.0, 0.1, 0.2, ..., 0.8, 0.9, 1.0) λ points, including 0.025, 0.05, 0.95, 0.975 (to smooth the integrand) in both the bound and unbound states. For the mutations in water, a 1 ns simulation was performed at each λ value. For the mutations in the protein, the system was first equilibrated for 0.2 ns, and 1.8 ns of sampling used to provide an initial estimate of $<\partial H/\partial\lambda>_\lambda$. In cases where the value of $<\partial H/\partial\lambda>_\lambda$ had not converged, the simulations were extended to 3 ns. To determine the degree of convergence, thermodynamic cycles wherein the molecules were transformed from one to another in circular path in water, and when bound to the protein, were constructed. The mutations were chosen in order to maximize the number of closed thermodynamic cycles that could be generated with a limited number of mutations. The degree of convergence was also checked by performing the forward and backward mutations. To prevent numerical instabilities as atoms were created or destroyed, the soft-core potential as described by Beutler et al.[35,36] was used with $\alpha_{LJ} = 0.5$ and $\alpha_C = 0.5$ nm^2. The area beneath the curve in (1) was estimated using a trapezoidal approximation. The error in $<\partial H/\partial\lambda>_\lambda$ was estimated using a block averaging procedure at each λ-point.[37] The individual errors were then integrated to yield an estimate of the error in ΔG. All mutations performed as part of this work are summarized in Table 3. All possible thermodynamic cycles that could be constructed from these mutations are shown diagrammatically in Figure 2.

Table 3. Change in the Gibbs FE for Mutations of Pairs of Inhibitors Listed in Figure *1* in Water and in PNMT

	ΔG(kJ/mol)				ΔG(kJ/mol)				ΔΔG (kJ/mol)		
	water				PNMT				PNMT−water		
mutation	forward[a]	backward[a]	|hysteresis|	average[b]	forward[a]	backward[a]	|hysteresis|	average[b]	$\Delta\Delta G_{calcd}$[c]	$\Delta\Delta G_{exp}$[d]	$\Delta\Delta G_{expt} - \Delta\Delta G_{calcd}$
1−2R	−372.4(1.2)	371.7(1.4)	0.7	−372.1 ± 1.4	−255.2(2.5)	268.1(2.2)	12.9	−261.7 ± 2.4	110.4 ± 2.8	–	–
1−2S	−371.9(1.6)	371.3(2.3)	0.6	−371.6 ± 2.0	−288.1(2.1)	297.3(1.7)	9.2	−292.7 ± 1.9	78.9 ± 2.8	–	–
1−3R	−5.5 (0.3)	5.1 (0.5)	0.4	−5.3 ± 0.4	−0.7(1.9)	1.2(1.2)	0.5	−1.0 ± 1.5	4.3 ± 1.6	–	–
1−3S	−5.5 (0.2)	5.3 (0.4)	0.2	−5.4 ± 0.3	−10.1(0.9)	10.6 (1.1)	0.5	−10.3 ± 1.0	−4.9 ± 1.0	–	–
1−4R	−3.2(1.3)	3.5(1.1)	0.3	−3.4 ± 1.2	−4.7(1.9)	4.3(1.0)	0.4	−4.5 ± 1.5	−1.1 ± 1.9	–	–
1−4S	−4.4(1.4)	4.7(0.4)	0.3	−4.6 ± 0.9	−9.1(0.4)	11.1(0.6)	2.0	−10.1 ± 0.5	−5.5 ± 1.0	–	–
1−5	6.2(0.6)	−6.1(0.9)	0.1	6.2 ± 0.8	−3.1(1.8)	4.0(1.5)	0.9	−3.5 ± 1.6	−9.7 ± 1.8	−10.8 ± 0.6	−1.1
1−6R	−39.2(0.8)	39.4(1.0)	0.2	−39.3 ± 0.9	−55.0(0.8)	52.2(1.1)	2.8	−53.6 ± 0.9	−14.3 ± 1.3	−14.6 ± 0.3	−0.3
1−6S	−37.2(0.7)	38.3(1.4)	1.1	−37.8 ± 1.0	−47.2(1.4)	48.9(2.4)	1.7	−48.1 ± 1.9	−10.3 ± 2.1	–	–
1−7	−342.8(1.4)	343.1(0.7)	0.3	−343.0 ± 1.1	−353.8(1.1)	355.2(1.7)	1.4	−354.5 ± 1.4	−11.5 ± 1.8	−9.7 ± 0.5	1.8
1−8R	−388.6(0.7)	388.7(0.9)	0.1	−388.7 ± 0.8	−397.9(1.3)	400.5(1.1)	2.7	−399.2 ± 1.2	−10.5 ± 1.4	−11.8 ± 0.3	−1.3
1−8S	−388.2(1.4)	387.9(0.8)	0.3	−388.1 ± 1.1	−397.8(0.8)	395.7(1.2)	2.1	−396.8 ± 2.0	−8.7 ± 2.3	–	–
1−9R	0.2(0.2)	−0.3(0.4)	0.5	0.2 ± 0.3	1.0(0.8)	−1.4(0.9)	0.4	1.2 ± 0.9	1.0 ± 1.0	–	–
1−9S	0.2(0.4)	−0.1(0.3)	0.3	0.2 ± 0.4	−12.4(1.8)	13.8(1.5)	1.4	−13.0 ± 1.7	−13.2 ± 1.7	–	–
1−10R	−124.2(0.9)	123.8(1.5)	0.4	−124.0 ± 1.2	−119.8(1.5)	122.2(2.1)	2.5	−121.0 ± 1.8	3.0 ± 2.2	–	–
1−10S	−123.2(1.4)	123.7(1.5)	0.5	−123.5 ± 1.5	−109.5(1.2)	112.2(1.8)	2.7	−110.9 ± 1.5	12.6 ± 2.1	–	–
1−11	−17.8(0.5)	17.9(0.6)	0.1	−17.8 ± 0.6	−33.9(0.7)	37.6(1.3)	3.7	−35.8 ± 1.0	−18.0 ± 1.2	−18.8 ± 0.4	−0.8
1−12R	−351.4(0.6)	351.8(0.8)	0.4	−351.6 ± 0.7	−362.3(2.3)	363.6(1.1)	1.3	−363.0 ± 1.7	−11.6 ± 1.8	–	–
1−12S	−351.2(0.7)	351.5 (0.3)	0.3	−351.6 ± 0.5	−353.1(1.2)	350.8(1.7)	2.3	−352.0 ± 1.4	−0.4 ± 1.5	–	–
2R−5	377.2(1.2)	−378.1(1.9)	0.9	377.7 ± 1.6	310.8(1.9)	–	–	–	−66.9 ± 2.5	–	–
2S−5	377.4(0.7)	−377.5(1.7)	0.1	377.5 ± 1.2	274.2(0.6)	−281.8 (1.6)	7.6	278.0 ± 1.1	−99.5 ± 1.6	–	–
2R−6R	332.0(1.6)	−331.8(0.9)	0.2	331.9 ± 1.3	286.6(2.3)	–	–	–	−46.3 ± 2.6	–	–
2S−6S	332.2(0.9)	−332.4(1.3)	0.2	332.3 ± 1.1	236.7(1.7)	−205.0(2.4)	31.7	220.9 ± 2.1	−111.4 ± 2.4	–	–
2R−9S	371.8(0.7)	−372.9(1.9)	1.1	372.4 ± 1.3	315.0(2.3)	–	–	–	−57.4 ± 2.6	–	–
2S−9R	372.2(0.4)	−372.7(1.4)	0.5	372.5 ± 0.9	272.2(2.3)	−252.0(1.4)	20.2	262.1 ± 1.9	−110.4 ± 2.1	–	–
3S−8R	−382.2(3.4)	382.1(1.4)	0.1	−382.2 ± 2.4	−398.2(2.6)	394.1(1.8)	4.1	−396.2 ± 2.2	−14.0 ± 3.2	–	–
3S−9S	6.2(0.6)	−6.1(1.1)	0.1	6.2 ± 0.9	−8.6(2.6)	8.0(1.2)	0.6	−8.3 ± 1.9	−14.5 ± 2.1	–	–
4R−7	−340.6(0.9)	340.2(1.3)	0.4	−340.4 ± 1.1	−353.7(2.1)	357.5(1.8)	3.8	−355.6 ± 2.0	−15.2 ± 2.3	–	–
4R−10S	−120.0(1.3)	120.0(0.8)	0.0	−120.0 ± 1.1	−103.3(1.5)	–	–	–	16.7 ± 1.8	–	–
5−6S	−44.5(1.5)	44.2(0.5)	0.3	−44.4 ± 1.0	−41.3(1.3)	41.2(2.2)	0.1	−41.3 ± 1.8	3.1 ± 2.1	–	–
5−9S	−6.2(0.5)	6.3(0.5)	0.1	−6.2 ± 0.5	−8.1(1.1)	8.5(1.3)	0.4	−8.3 ± 1.2	−2.1 ± 1.3	–	–
6S−10S	−84.2(1.3)	85.1(0.6)	0.9	−84.7 ± 1.0	−69.8(2.2)	65.8(1.7)	4.0	−67.5 ± 2.0	17.2 ± 2.2	–	–
7−8S	−44.7(0.4)	45.2(0.8)	0.5	−45.0 ± 0.6	−45.8(1.9)	–	–	–	−0.8 ± 2.0	–	–

[a] The values in the parentheses show the standard error estimate obtained by block averaging. [b] The standard error in the average column were calculated by $[(s_1)^2 + (s_2)^2/2]^{1/2}$, where s_1 and s_2 are the standard error for the forward and backward mutations, respectively. [c] The error for the $\Delta\Delta G_{calcd}$ (PNMT−water) was calculated by formula $[(s_1)^2 + (s_2)^2]^{1/2}$, where s_1 and s_2 are the standard error for the mutations in water and PNMT, respectively. [d] Where multiple values for the FE of binding are available only the values obtained from refs 16, 21, 23, 24, and 26 shown as bold italics in Table 1 were used as these were the most recently available at the time of publication.

RESULTS AND DISCUSSION

MD Simulation of Ligand−PNMT Complexes. To examine if the system was equilibrated and if the ligand−PNMT complexes were stable in the force field used, the atomic positional root-mean-square deviation (rmsd) of the protein bound to inhibitor **7** with respect to initial X-ray crystal structure (pdb code 1HNN) was calculated. The average rmsd value with respect to the starting structure equilibrates after approximately 2 ns of simulation at 0.2 nm for the backbone atoms and 0.25 nm for all atoms, respectively, with the interactions between ligand and binding site remaining essentially the same as that proposed in the X-ray crystal structure. The aromatic ring of the THIQ nucleus is involved in a π-stacking arrangement with the side chain of Phe181. The ring N of THIQ formed a salt bridge with the side chain carboxylate of Glu219 and the water-mediated hydrogen bond with the side chain O of Asn39 and side chain O of Asp267. Almost all of the other ligands showed a similar degree of stability and similar interactions with PNMT. The exceptions were the molecules **2R** and **2S**. Molecules **2R** and **2S**, which are very weak inhibitors (>2000 μM), cannot adopt the same binding mode as the other ligands due to the fact molecule **2** has a charged carboxylate group and will be discussed in detail later.

Convergence of the Free Energy Calculations in Water and Bound to PNMT. The degree of convergence in the FE calculations was monitored in two ways. Out of the 33 pairs of mutations investigated, 28 pairs were performed in both the forward and the backward directions (Table 3). In addition, thermodynamic cycles in water and in the protein were constructed as described in the Methods Section. As the FE is a state function, the FE for the forward and backward mutations should be identical except for the sign. In addition, the FE for any closed cycle should be zero. Figure 2 shows all possible thermodynamic cycles for the different mutations performed in water and PNMT. All possible three-membered thermodynamic cycles that can be constructed from Table 3 are listed in Table 4. Using the mean of the FE in the forward and backward directions all three-membered cycles in water close to within 1.1 kJ/mol. The convergence of the forward and backward transformations in

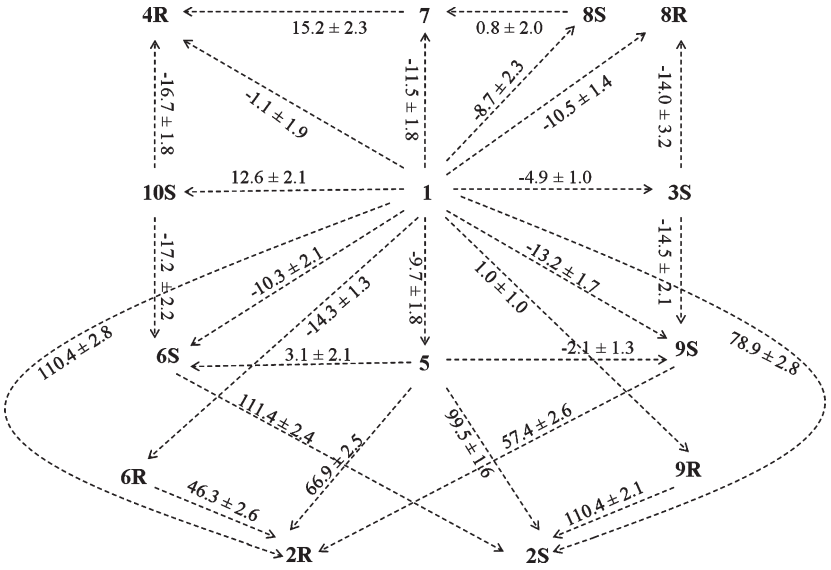

Figure 2. Schematic showing all possible closed thermodynamic cycles can be built from the mutations listed in Table 3. Note that the arrows refer the mutation performed in a given direction. The values listed on each line correspond to the difference in the average FE values between PNMT and water for these mutations.

Table 4. All Possible Three-Memebered Thermodynamic Cycles That Can Be Constructed from Table 3

thermodynamic cycles	water ΔG^a (kJ/mol)[b]	PNMT ΔG^a (kJ/mol)[b]	PNMT−water $\Delta\Delta G^a$ (kJ/mol)[c]
1→2R→5→1	−0.6 ± 2.3	186.4 ± 3.5	187.0 ± 4.1
1→2R→6R→1	−0.9 ± 2.1	77.5 ± 3.4	78.4 ± 4.0
1→2S→5→1	−0.3 ± 2.5	−11.2 ± 2.7	−10.9 ± 3.7
1→2S→9R→1	0.7 ± 2.2	−31.8 ± 2.8	−32.5 ± 3.6
1→3S→8R→1	1.1 ± 2.5	−7.3 ± 2.7	−8.4 ± 3.7
1→3S→9S→1	0.6 ± 1.0	−5.6 ± 2.7	−6.2 ± 2.9
1→4R→10S→1	0.3 ± 2.2	3.3 ± 2.6	3.0 ± 3.4
1→5→9S→1	−0.2 ± 1.0	1.2 ± 2.6	1.4 ± 2.8
1→6S→5→1	0.4 ± 1.4	−3.3 ± 3.1	−3.7 ± 3.7
1→7→4R→1	0.8 ± 2.0	5.6 ± 2.9	4.8 ± 3.5
1→7→8S→1	0.0 ± 1.7	−3.6 ± 3.1	−3.6 ± 3.5
1→9S→2R→1	−0.1 ± 2.0	−66.3 ± 3.7	−66.2 ± 4.2
1→10S→6S→1	−1.0 ± 2.1	4.7 ± 3.1	5.7 ± 3.8
5→6S→2S→5	0.8 ± 1.8	15.8 ± 3.0	15.0 ± 3.5
5→9S→2R→5	−0.9 ± 2.1	121.3 ± 3.2	122.2 ± 3.9

[a] The residual FE averaged for the forward and backward mutations for each leg in water and in PNMT and for the difference between water and PNMT is shown. [b] The errors were calculated by formula $[(s_1)^2 + (s_2)^2 + (s_3)^2]^{1/2}$ where s_1, s_2, and s_3 are the standard errors for the three different legs for mutations in water and PNMT. [c] The errors for $\Delta\Delta G$ were calculated by $[(s_1)^2 + (s_2)^2]^{1/2}$, where s_1 and s_2 are the standard errors for cycles in water and PNMT, respectively.

water is illustrated in Figure 3, which show plots of $<\partial H/\partial\lambda>$ versus λ for selected mutations. Figure 3a shows the forward and backward mutations for the transformation of molecule **1** to **3R** and molecule **1** to **3S**. As shown in Figure 3a, there is an almost perfect overlap in the value of $<\partial H/\partial\lambda>$ for all λ values for the forward and backward mutations for both **1** to **3R** and **1** to **3S** as expected. Comparable results were obtained in all other cases with the difference in FE for the forward and backward mutations (hysteresis) in water being ≤1.1 kJ/mol, demonstrating that the calculations in water were well converged.

From Table 4 it can be seen that taking the average between the forward and backward mutations, all cycles not involving **2R** and **2S** in PNMT converged to within 7.3 kJ/mol, with the average residual being 4.3 kJ/mol. While clearly the results in PNMT are not as well converged as in water, the intrinsic error in most cases is still low. The convergence of the forward and backward transformations is illustrated in Figure 3b, which shows a plot of $<\partial H/\partial\lambda>$ versus λ for the forward and backward mutations for the transformation of molecule **1** to **3R** and molecule **1** to **3S** in PNMT. Again there is an almost perfect overlap in the value of $<\partial H/\partial\lambda>$ for all λ values for the forward and backward mutations in both cases. Note, the change in FE for the mutations **1**−**3R** and **1**−**3S** in water (Figure 3a) are essentially identical as required. From Figure 3b it can be seen there is a significant difference between the mutations **1**−**3R** and **1**−**3S** when bound to PNMT, reflecting enantiomeric selective

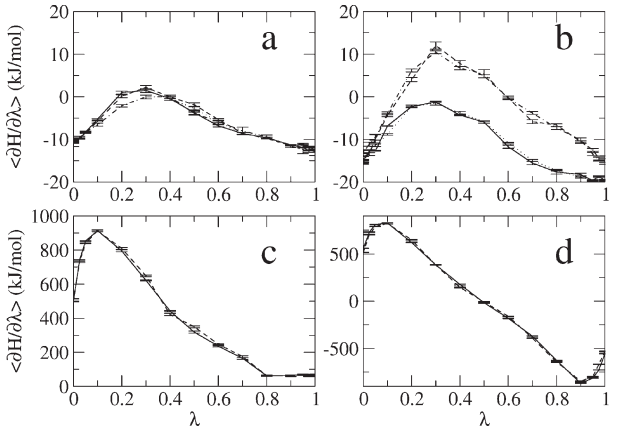

Figure 3. FE profiles for the mutation of specific inhibitors in water and in PNMT. Each graph shows the value of the integrand $<\partial H/\partial\lambda>_\lambda$ at each λ-value. The error bars correspond to the standard error of $\partial H/\partial\lambda$ at each λ-value. (a) Mutation of **1**→**3R** (solid line), **3R**→**1** (dashed line), **1**→**3S** (dots), and **3S**→**1** (dots and dashed line) in water; (b) mutation of **1**→**3R** (solid line) and **1**→**3S** (dashed line) in PNMT; (c) mutation of **8R**→**3S** (solid line) and **3S**→**8R** (dashed line) in PNMT; (d) mutation of the inhibitor **13S** from the binding mode proposed in pdb 2AN5 to the binding mode of the substrate **13R** in pdb 2AN3. All values are in kJ/mol.

binding. The failure of the cycle **1**−**3S**−**8R**−**1** to close within 7.3 ± 4.4 kJ/mol is primarily due to the high hysteresis between the forward and backward calculations for the mutation **3S**−**8R** (Table 3). The mutation **3S**−**8R** has a hysteresis of 4.1 kJ/mol. Figure 3c shows a plot of $<\partial H/\partial\lambda>$ versus λ for the forward and backward mutations for **3S**−**8R**. Even in this case there is still almost perfect overlap between the forward and backward mutations for each λ value, with the intrinsic error being less than 0.5% of the value of $<\partial H/\partial\lambda>_\lambda$ at $\lambda = 0.1$.

The three-membered thermodynamic cycles in PNMT involving the molecules **2R** and **2S** have an error ranging from ∼11 kJ/mol to as high as ∼186 kJ/mol based on the average of the forward and backward mutations for each leg. Clearly the calculations involving molecules **2R** and **2S** have not converged. This is also reflected in the high hysteresis between the forward and backward mutations involving **2R** and **2S** (Table 3). Experimental binding data are only available for a racemic mixture of molecule **2** against the bovine PNMT. This suggests that both **2R** and **2S** bind only weakly. In the MD simulations of the human PNMT−**2R** and PNMT−**2S** complexes, the binding modes of **2R** and **2S** are unstable, suggesting that they have very low affinity for human PNMT and explaining why the calculations are poorly converged.

Comparison to Experiment. In order to compare the calculated differences in the FE of binding between the different THIQ derivatives to the available experimental data, a series of thermodynamic cycles were constructed. Note in this system, the validation of the results from the simulations by comparison to experiment is complicated by several factors. Table 1 shows there are large differences in the experimental estimates reported by different authors with a range of values for the binding affinity of specific inhibitors having been published even by the same group.[22,23] For example, the variation in the experimental estimate of the binding FE is in the order of ∼2 kJ/mol for molecule **1**, ∼4 kJ/mol for molecule **7**, ∼9 kJ/mol for molecule **8R**, and ∼11 kJ/mol for molecule **11**. This is despite the fact that

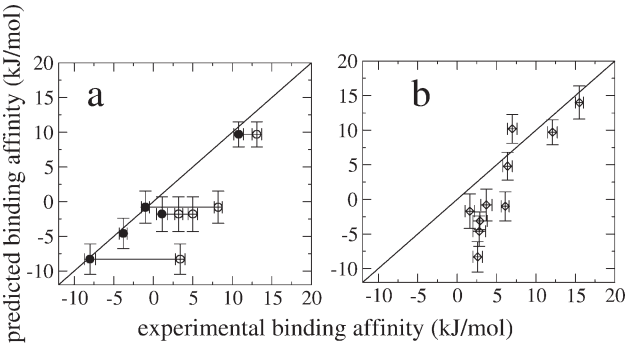

Figure 4. Plot of the experimental versus the calculated binding affinities in kJ/mol (relative to inhibitor **5**). The straight diagonal line has a slope of 1.0 and corresponds to a perfect correlation between the calculated and the experimental values. The vertical lines show the error in the calculated FE values. (a) Comparison with human PNMT, the horizontal lines connect different experimental values for one compound, the filled circles show the recent experimental binding data, the open circle shows the earlier experimental binding data; and (b) comparison with bovine PNMT.

the error in any of the individual values was claimed to be less than 1.0 kJ/mol. Also in some cases experimental binding data are only available for the bovine PNMT and usually for one isomer in the case of human PNMT.

Table 3 shows a direct comparison between the mutations performed and the experimental relative binding FE. Specifically, column 12 of Table 3 lists the difference between the FE of binding determined experimentally and the FE of binding estimated from the FE calculations for individual mutations for which a one-to-one comparison in human PNMT can be made. As can be seen, there is an almost exact correlation between the calculated and the experimental free energies for the inhibitors binding to human PNMT based on the most recent human PNMT data highlighted in bold italics in Table 1. The average absolute deviation is 1.0 kJ/mol with the maximum deviation of 1.8 kJ/mol in the case of molecule **7**.

In order to compare the calculated relative binding free energies to all the available experimental data for both human and bovine PNMT, the relative binding free energies with respect to inhibitor **5** were calculated. Inhibitor **5**, which is achiral and conformationally rigid, was selected as a reference as only one experimental K_i value for human PNMT has been published. The last column of Table 1 shows the difference between the calculated and the experimental values for the FE of binding relative to inhibitor **5** ($\Delta\Delta G_{expt} - \Delta\Delta G_{calcd}$). Again it can be seen there is an almost one-to-one correspondence between the calculated and the most recent experimental estimates of the inhibitors binding to human PNMT. Figure 4a shows a plot of the calculated and the various experimental values for the relative binding FE of the available THIQ derivatives to human PNMT. In Figure 4a, the filled circles indicate the most recent experimental estimates, whereas the open circles connected by the horizontal lines correspond to earlier experimental estimates. Note, even in the case of molecule **7**, there is a progressive convergence of the experimental estimate of binding affinity toward the calculated value with time. The binding affinity of molecule **7** for human PNMT was estimated to be 0.58 ± 0.04 μM (−35.9 ± 0.2 kJ/mol) by Grunewald et al.[22] in 2001, 0.28 ± 0.02 μM (−37.7 ± 0.1 kJ/mol) by Wu et al.[23,27] in 2004 (quoting earlier values of Pendleton et al.),[27] and 0.12 ± 0.02 μM (−39.8

± 0.3 kJ/mol) by Wu et al.[21,26] in 2005. A partial explanation for this variation is that earlier estimates were obtained using low concentrations of the cofactor and PNMT and also the possible contamination of the cofactor.[23] This not only highlights the predictive power of the FE calculations but also the pressing need for reliable experimental data against which computational models can be validated. In this case any comparison to data published earlier this decade would have led to the incorrect assumption that the FE calculations were not predictive. In reality the uncertainty in the calculations in this case is much less than the variation in the experimental values over time.

Another point worth noting is that much of the analysis of the binding of THIQ inhibitors to PNMT is based on an analysis of binding data obtained using the bovine enzyme. In fact for many of the compounds listed in Table 1, experimental data are only publically available for the bovine form. Despite the very high sequence identity between the human and bovine forms of the enzyme of 84%, it is known that, while certain compounds may have similar binding affinities between the human and the bovine forms of the enzyme in other cases such as molecules **6R**, **8R** and **11**, the values differ markedly.[19,22,24,25] Figure 4b shows a plot of the calculated relative binding free energies in human PNMT versus the values for bovine PMNT reported in the literature. Based on the calculations we would predict that molecules **1**, **2R**, **2S**, **3R**, **3S**, **7**, **9R**, and **12R** will have similar binding affinities (<4 kJ/mol) to both the human and the bovine forms of the enzyme, whereas molecules **4R**, **4S**, **6R**, **8R**, **10R**, **10S**, and **11** would have a significantly higher affinity (>6 kJ/mol) for the human as compared to the bovine form. Note, no X-ray crystallographic structure of bovine PNMT is currently available.

Enantiomeric Selectivity. Experimental binding data related to the enantiomeric selectivity of the THIQ derivatives considered in this study toward PNMT are only available for the bovine form of the enzyme. The calculations nevertheless correctly predict the relative binding FE of the enantiomers in all cases for which experimental data is available. The FE calculations predict that PNMT preferentially binds **3S** over **3R** by ~9 kJ/mol. The calculations also correctly predict the preferential binding of **6R** over **6S** by ~8 kJ/mol and preferential binding of **9S** over **9R** by ~12 kJ/mol. For the other molecules in the test set there is no data for both enantiomers, and for three molecules (**2**, **4**, and **10**), experimental binding data for bovine PNMT are only available for racemic mixtures. The calculations predict that human PNMT would preferentially bind molecule **4S** over **4R** by ~4 kJ/mol and **8R** over **8S** by ~2 kJ/mol, and thus the enzyme shows only weak enantiomeric selectivity to these compounds. However, the calculation would predict that human PNMT would preferentially bind molecule **10R** over **10S** and molecule **12R** over **12S** by more than 10 kJ/mol in each case.

Structure−Activity Relationships (SAR). In the current work, the FE of binding for 20 analogues of THIQ interacting with human PNMT has been derived with enantiomeric selective data being derived for eight of these compounds. This provides an opportunity to analyze possible structure−activity relationships. As noted previously, electron-withdrawing polar substituents (−NO_2, −SO_2NH_2, and −Cl) at the seven position of the THIQ ring enhance binding affinity toward human PNMT at least by ~10 kJ/mol (compared to THIQ, molecule **1**). An additional −Cl substituent at position eight of THIQ (**11**) improves the binding affinity by a further 10 kJ/mol. Based on this we would predict that the addition of a small electron-withdrawing group at position eight may be an effective means to increase the affinity of THIQ derivatives toward human PNMT. It is also clear that the stereochemistry at position three plays an important role in determining the binding affinity. From Table 1 it can be seen that for nonpolar substituents, such as −CH_3 (**3**, **9**) and −C_2H_5 (**4**), the '*S*' enantiomer binds preferentially, while in the case of the polar substituents, such as −CH_2OH (**6**, **8**), −$COOCH_3$ (**10**), and −CH_2F (**12**), the '*R*' enantiomer is preferred. It is important to note, however, that in terms of absolute stereochemistry the preferred compounds are those in which substituent at the three position lies equatorial with respect to the piperidine ring projecting toward Tyr222 with the nitrogen of the ring forming a salt bridge with the side chain of Glu219. In the other enantiomer, if the salt bridge to Glu219 is maintained, then the substituent at position three would lie axial to the ring and project toward the backbone of Phe182, which could explain the lower affinity. However, the overall affinity depends on competing interactions that cannot easily be reduced to a simple structure−activity relationship, such as the size or the hydrophobicity of the substituent at position three. This is illustrated by the fact that while compounds **3**, **9**, and **12**, which have only a small substituent at position three (−CH_3 or −CH_2F), and molecule **10**, which has the largest substituent at position three (−$COOCH_3$), show good enantiomeric selectivity, and intermediate size substituents (−C_2H_5 and −CH_2OH) are predicted to show only weak selectivity.

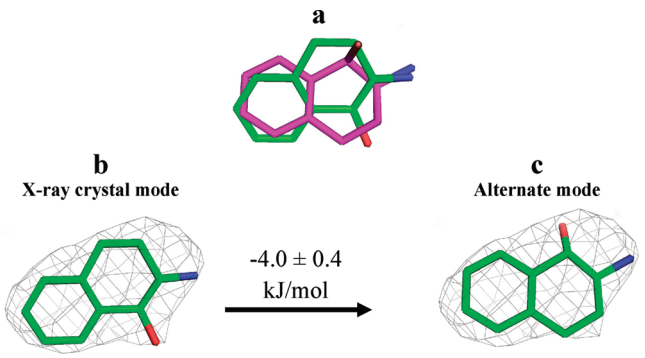

Figure 5. (a) The binding mode of substrate **13R** (magenta) inhibitor **13S** (green) as proposed in the X-ray crystal structure pdb code 2AN3 and 2AN5, respectively. 2Fo−Fc map contoured at 1.0σ for inhibitor **13S** in (b) pdb code 2AN5 and (c) alternate binding mode, which is similar to substrate **13R**.

Binding of Chiral 2-Amino-1-tetralol to PNMT. Stereochemistry also plays an important role in the recognition of other PNMT ligands.[38] For example, compound **13R** and **13S**, which are epimers (diastereoisomers with the opposite stereochemistry at one of the chiral centers), behave very differently when bound to PMNT. The compound **13R** is a substrate for PNMT, whereas **13S** acts as an inhibitor. The X-ray crystallographic models of Gee et al. suggested that the two compounds have different modes of binding (Figure 5a, pdb code 2AN3 and 2AN5) and used this to explain their different biochemical behavior.[38] Specifically it was proposed that the inhibitor **13S** binds in an orientation that is rotated by 180° to the long axis of the fused ring when compared to the substrate **13R** (Figure 5a).

In order to investigate the validity of this proposal, MD simulations of **13R** and **13S** in both the proposed binding modes were performed beginning from pdb structures 2AN3 and 2AN5. In case of **13R** the proposed X-ray binding mode was stable, whereas the alternate binding mode resulted in the disruption of

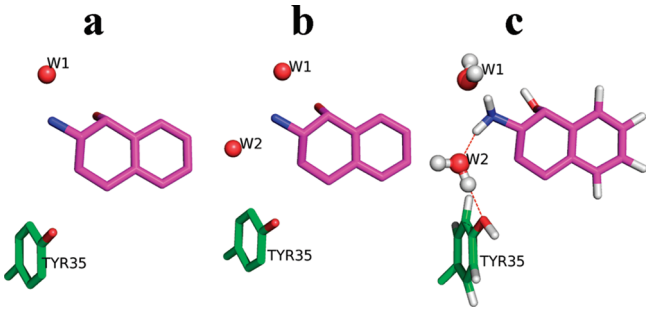

Figure 6. The crystal structure of substrate **13R** complexed with PNMT: (a) molecule A of the asymmetric unit with water, W1 and (b) molecule B of the asymmetric unit with water W1 and W2. (c) The $-NH_3^+$ of substrate **13R** shows water-mediated (W2) hydrogen-bond interaction (red, dotted line) with Tyr35 observed in MD simulation.

active site. In case of **13S**, while the proposed X-ray crystal mode was stable, the alternate binding mode was equally stable (Figure 5c). In fact, as shown in Figure 5b and c, both orientations fit equally well within the experimental electron density. In such cases one cannot easily distinguish the preferred binding mode based on the density, geometry, or energetic criteria or on the global indicators of quality, such as R and R_{free}.[5] In such cases one must instead turn to FE approaches to determine which of the two modes is the more thermodynamically stable. The calculations suggest that the preferred binding mode of the inhibitor **13S** is the same as that of the substrate **13R** with the alternative binding mode proposed in the X-ray structure being higher in FE by ~4 kJ/mol. Again as can be seen from Figure 3d, there was an almost perfect overlap of forward and backward transformations between X-ray crystal and alternate modes of **13S** in PNMT, indicating the calculations were very well converged. Again, the difference in FE, which corresponds to a factor of 5 in the binding affinity, is much greater than the uncertainty in the calculations.

The Role of Water in Ligand Binding. The crystallographic model of the **13R**−PNMT complex (pdb code 2AN3, resolution 2.20 Å) has two molecules (A and B) in the asymmetric unit. Molecule A contains a single structural water molecule (W1, Figure 6a), while molecule B contains two structural water molecules (W1 and W2, Figure 6b) in the binding pocket. To determine whether these water molecules were critical to maintain the stability of the active site, separate simulations of both A and B were performed. In the case of molecule A, an additional water molecule entered the pocket forming hydrogen bonds with the $-NH_3^+$ group of the ligand and the −OH group of Tyr35, as shown in Figure 6c, and remained stable in this position throughout the simulation. In the case of molecule B, the second structural water molecule, W2, occupied at the same position (Figure 6c) as described earlier. This suggests that the water molecule W2 is required to maintain the interaction between PNMT and **13R** as observed in the crystal structure.

Experimentally the mutation of Tyr35Phe shows a substantial decrease in the binding affinity for **13R** and the cofactor *S*-adenosyl-L-methionine (SAM).[38] The reduction in the binding affinity for the cofactor can be understood in terms of the interaction of the Tyr35 hydroxyl group with the carboxylate oxygen of the amino acid fragment of the cofactor analogue SAH used in crystallization. However, it was not clear why the binding affinity of the substrate **13R** was also affected by Tyr35Phe mutation.[38] In the simulations, W2 forms a water-mediated interaction between **13R** and the hydroxyl group of Tyr35, and it is likely that this accounts for the reduction in the binding affinity of the substrate when Tyr35 is mutated to Phe.

CONCLUSIONS

In this work the stereospecific binding affinity for a series of 20 analogues of THIQ and the stereospecific binding mode of 2-amino-1-tetralol to human PNMT have been investigated. Specifically, molecular dynamics simulations and free energy calculations have been used to understand in detail the structural and thermodynamic basis of ligand recognition in this system. This is an important case study as the binding affinities proposed by different sets of workers in different studies differ significantly and revised values based on new assay conditions have been recently published. For those THIQ analogues for which recent experimental data are available, excellent agreement between calculated and measured relative binding free energies to human PNMT was obtained. The average deviation between the calculated and the experimentally determined values for these compounds using molecule **5** as a reference was only 0.8 kJ/mol, showing that the calculations can easily distinguish between the data sets. This highlights the fundamental challenge when attempting to compare theoretical calculations to measured binding affinities and the critical need for reliable and validated experimental data.[39] Clearly, the variation in the published experimental data (despite the small errors claimed for each of the individual experimental observations) is much greater than the intrinsic uncertainty in the theoretical estimates.

The calculations have also enabled a detailed analysis of the structure−activity relationships of these THIQ analogues. In particular, the addition of a small electron-withdrawing group at position eight is predicted to be an effective means to increase the affinity of THIQ derivatives toward human PNMT. It is also evident that the relative orientation of the substituents rather than absolute stereochemistry at position three of THIQ appears to govern enantiomeric selectivity. The size of the group at position three of THIQ also plays a nontrivial role in enantiomeric selectivity with small substituents, such as a methyl or fluoromethyl group, showing greater enantiomeric selectivity than slightly larger groups, such as ethyl and hydroxmethyl. In case of **13R**, the importance of the role specific structural waters can play in ligand recognition has been illustrated. For example, interactions between the substrate **13R** and Tyr35 involving a specific structural water (W2) can explain the effect of mutations at position 35 on enzymatic activity. Finally, the thermodynamically stable binding mode in case of the inhibitor **13S** is predicted to be similar to that of the substrate **13R** as opposed to the novel binding mode proposed in the pdb entry 2AN5. Overall the work highlights the power of MD simulations and the free energy calculations to resolve uncertainties in experimental binding affinities, binding modes, and other aspects related to X-ray refinement and computational drug design.

AUTHOR INFORMATION

Corresponding Author

*E-mail: a.e.mark@uq.edu.au.

ACKNOWLEDGMENT

P.C.N. acknowledges the Australian government and the University of Queensland for the award of an Endeavour

International Postgraduate Research Scholarship (IPRS), A.K.M. acknowledges Australian Research Council (ARC; grant no. DP 0987043) for the award of an Australian Post-Doctoral (APD) fellowship. Computational resources were provided by the National Computational Infrastructure (NCI, Australia) projects m72 and n63. The authors would like to thank the reviewers for their comments and suggestions to improve the quality of the paper.

REFERENCES

(1) Verlinde, C. L. M. J.; Hol, W. G. J. Structure-based drug design: progress, results and challenges. *Structure* **1994**, *2*, 577–587.

(2) Karplus, P. A.; Faerman, C. Ordered water in macromolecular structure. *Curr. Opin. Struct. Biol.* **1994**, *4*, 770–776.

(3) Kollman, P. Free energy calculations: Applications to chemical and biochemical phenomena. *Chem. Rev.* **1993**, *93*, 2395–2417.

(4) Malde, A. K.; Mark, A. E. Binding and enantiomeric selectivity of threonyl-tRNA synthetase. *J. Am. Chem. Soc.* **2009**, *131*, 3848–3849.

(5) Malde, A. K.; Mark, A. E. Challenges in the determination of the binding modes of non-standard ligands in X-ray crystal complexes. *J. Comput.-Aided. Mol. Des.* **2011**, *25*, 1–12.

(6) Ziegler, M. G.; Kennedy, B.; Elayan, H. Extraadrenal adrenaline formation by two separate enzymes. *Cell. Mol. Life Sci.* **1989**, *45*, 718–720.

(7) Hökfelt, T.; Fuxe, K.; Goldstein, M.; Johansson, O. Immunohistochemical evidence for the existence of adrenaline neurons in the rat brain. *Brain Res.* **1974**, *66*, 235–251.

(8) Crowley, W. R.; Terry, L. C.; Johnson, M. D. Evidence for the involvement of central epinephrine systems in the regulation of luteinizing hormone, prolactin, and growth hormone release in female rats. *Endocrinology* **1982**, *110*, 1102–1107.

(9) Fuller, R. W.; Roush, B. W. Substrates and inhibitors of phenyletholamine n-methyl transferase from human adrenal glands. *Int. J. Biochem.* **1972**, *3*, 225–228.

(10) Fuller, R. W.; Roush, B. W.; Snoddy, H. D.; Day, W. A.; Molloy, B. B. Norepinephrine N-methyltransferase inhibition by benzamidines, phenylacetamidines, benzylguanidines, and phenylethylguanidines. *J. Med. Chem.* **1975**, *18*, 304–307.

(11) Grunewald, G. L.; Caldwell, T. M.; Li, Q.; Criscione, K. R. Synthesis and evaluation of 3-trifluoromethyl-7-substituted- 1,2,3,4-tetrahydroisoquinolines as selective inhibitors of phenylethanolamine N-methyltransferase versus the α2-Adrenoceptor. *J. Med. Chem.* **1999**, *42*, 3315–3323.

(12) Grunewald, G. L.; Dahanukar, V. H.; Ching, P.; Criscione, K. R. Effect of ring size or an additional heteroatom on the potency and selectivity of bicyclic benzylamine-type inhibitors of phenylethanolamine N-methyltransferase. *J. Med. Chem.* **1996**, *39*, 3539–3546.

(13) Toomey, R. E.; Horng, J. S.; Hemrick-Luecke, S. K.; Fuller, R. W. α2-Adrenoceptor affinity of some inhibitors of norepinephrine N-methyltransferase. *Life Sci.* **1981**, *29*, 2467–2472.

(14) Grunewald, G. L.; Romero, F. A.; Criscione, K. R. Nanomolar inhibitors of CNS epinephrine biosynthesis: (R)-(+)-3-fluoromethyl-7-(N-substituted aminosulfonyl)-1,2,3,4-tetrahydroisoquinolines as potent and highly selective inhibitors of phenylethanolamine N-methyltransferase. *J. Med. Chem.* **2004**, *48*, 1806–1812.

(15) Grunewald, G. L.; Romero, F. A.; Criscione, K. R. 3-Hydroxymethyl-7-(N-substituted aminosulfonyl)-1,2,3,4-tetrahydroisoquinoline Inhibitors of phenylethanolamine N-methyltransferase that display remarkable potency and selectivity. *J. Med. Chem.* **2004**, *48*, 134–140.

(16) Romero, F. A.; Vodonick, S. M.; Criscione, K. R.; McLeish, M. J.; Grunewald, G. L. Inhibitors of phenylethanolamine N-methyltransferase that are predicted to penetrate the blood-brain barrier: design, synthesis, and evaluation of 3-fluoromethyl-7-(N-substituted aminosulfonyl)-1,2,3,4-tetrahydroisoquinolines that possess low affinity toward the α2-adrenoceptor. *J. Med. Chem.* **2004**, *47*, 4483–4493.

(17) Grunewald, G. L.; Caldwell, T. M.; Li, Q.; Criscione, K. R. 1,3-Dimethyl-7-substituted-1,2,3,4-tetrahydroisoquinolines as probes for the binding orientation of tetrahydroisoquinoline at the active site of phenylethanolamine N-methyltransferase. *Bioorg. Med. Chem.* **1999**, *7*, 869–880.

(18) Grunewald, G. L.; Dahanukar, V. H.; Criscione, K. R. Effects of a 3-alkyl-, 4-hydroxy- and/or 8-aromatic-substituent on the phenylethanolamine N-methyltransferase inhibitor potency and [alpha]2-adrenoceptor affinity of 2,3,4,5-tetrahydro-1H-2-benzazepines. *Bioorg. Med. Chem.* **2001**, *9*, 1957–1965.

(19) Grunewald, G. L.; Dahanukar, V. H.; Teoh, B.; Criscione, K. R. 3,7-Disubstituted-1,2,3,4-tetrahydroisoquinolines display remarkable potency and selectivity as inhibitors of phenylethanolamine N-methyltransferase versus the α2-Adrenoceptor. *J. Med. Chem.* **1999**, *42*, 1982–1990.

(20) Begun, J.; McLeish, M. J.; Caine, J. M.; Palant, E.; Grunewald, G. L.; Martin, J. L. Crystallization of PNMT, the adrenaline-synthesizing enzyme, is critically dependent on a high protein concentration. *Acta Cryst. D* **2002**, *58*, 314–315.

(21) Gee, C. L.; Drinkwater, N.; Tyndall, J. D. A.; Grunewald, G. L.; Wu, Q.; McLeish, M. J.; Martin, J. L. Enzyme adaptation to inhibitor binding: A cryptic binding site in phenylethanolamine N-methyltransferase. *J. Med. Chem.* **2007**, *50*, 4845–4853.

(22) Grunewald, G. L.; McLeish, M. J.; Criscione, K. R. Phenylethanolamine N-methyltransferase kinetics: bovine versus recombinant human enzyme. *Bioorg. Med. Chem. Lett.* **2001**, *11*, 1579–1582.

(23) Wu, Q.; Criscione, K. R.; Grunewald, G. L.; McLeish, M. J. Phenylethanolamine N-methyltransferase inhibition: re-evaluation of kinetic data. *Bioorg. Med. Chem. Lett.* **2004**, *14*, 4217–4220.

(24) Grunewald, G. L.; Seim, M. R.; Regier, R. C.; Martin, J. L.; Gee, C. L.; Drinkwater, N.; Criscione, K. R. Comparison of the binding of 3-fluoromethyl-7-sulfonyl-1,2,3,4-tetrahydroisoquinolines with their isosteric sulfonamides to the active site of phenylethanolamine N-methyltransferase. *J. Med. Chem.* **2006**, *49*, 5424–5433.

(25) Grunewald, G. L.; Sall, D. J.; Monn, J. A. Synthesis and evaluation of 3-substituted analogs of 1,2,3,4-tetrahydroisoquinoline as inhibitors of phenylethanolamine N-methyltransferase. *J. Med. Chem.* **1988**, *31*, 824–830.

(26) Wu, Q.; Gee, C. L.; Lin, F.; Tyndall, J. D.; Martin, J. L.; Grunewald, G. L.; McLeish, M. J. Structural, mutagenic, and kinetic analysis of the binding of substrates and inhibitors of human phenylethanolamine N-methyltransferase. *J. Med. Chem.* **2005**, *48*, 7243–7252.

(27) Pendleton, R. G.; Gessner, G.; Weiner, G.; Jenkins, B.; Sawyer, J.; Bondinell, W.; Intoccia, A. Studies on SK&F 29661, an organ-specific inhibitor of phenylethanolamine N-methyltransferase. *J. Pharmacol. Exp. Ther.* **1979**, *208*, 24–30.

(28) van Gunsteren, W. F.; Billeter., S. R.; Eising, A. A.; Hünenberger, P. H.; Krüger, P.; Mark, A. E.; Scott, W. R. P.; Tironi, I. G. *Biomolecular Simulations: The GROMOS96 Manual and User Guide*; Swiss Federal Institute of Technology Zurich: Zurich, Switzerland, 1996.

(29) Oostenbrink, C.; Villa, A.; Mark, A. E.; Van Gunsteren, W. F. A biomolecular force field based on the free enthalpy of hydration and solvation: The GROMOS force-field parameter sets 53A5 and 53A6. *J. Comput. Chem.* **2004**, *25*, 1656–1676.

(30) Malde, A. K.; Zuo, L.; Breeze, M.; Stroet, M.; Poger, D.; Nair, P. C.; Oostenbrink, C.; Mark, A. E. An Automated force field Topology Builder (ATB) and repository: version 1.0. *J. Chem. Theory Comput.*, manuscript submitted.

(31) Berendsen, H. J. C.; Postma, J. P. M.; van Gunsteren, W. F.; Hermans, J. Interaction models for water in relation to protein hydration. In *Intermolecular Forces*, Pullman, B., Ed. Reidel: Dordrecht, 1981; pp 331−342.

(32) Berendsen, H. J. C.; Postma, J. P. M.; van Gunsteren, W. F.; DiNola, A.; Haak, J. R. Molecular dynamics with coupling to an external bath. *J. Chem. Phys.* **1984**, *81*, 3684–3690.

(33) Ryckaert, J.; Ciccotti, G.; Berendsen, H. Numerical integration of the cartesian equations of motion of a system with constraints: molecular dynamics of n-alkanes. *J. Comput. Phys.* **1977**, *23*, 327–341.

(34) Martin, J. L.; Begun, J.; McLeish, M. J.; Caine, J. M.; Grunewald, G. L. Getting the adrenaline going: Crystal structure of the adrenaline-synthesizing enzyme PNMT. *Structure* **2001**, *9*, 977–985.

(35) Beutler, T. C.; Mark, A. E.; van Schaik, R. C.; Gerber, P. R.; van Gunsteren, W. F. Avoiding singularities and numerical instabilities in free energy calculations based on molecular simulations. *Chem. Phys. Lett.* **1994**, *222*, 529–539.

(36) Zacharias, M.; Straatsma, T. P.; McCammon, J. A. Separation-shifted scaling, a new scaling method for Lennard-Jones interactions in thermodynamic integration. *J. Chem. Phys.* **1994**, *100*, 9025–9031.

(37) Allen, M. P.; Tildesley, D. J. *Computer Simulations of Liquids*. Clarendon Press: Oxford, U.K., 1987.

(38) Gee, C. L.; Tyndall, J. D. A.; Grunewald, G. L.; Wu, Q.; McLeish, M. J.; Martin, J. L. Mode of binding of methyl acceptor substrates to the adrenaline-synthesizing enzyme phenylethanolamine N-methyltransferase: Implications for catalysis. *Biochemistry* **2005**, *44*, 16875–16885.

(39) van Gunsteren, W. F.; Dolenc, J.; Mark, A. E. Molecular simulation as an aid to experimentalists. *Curr. Opin. Struct. Biol.* **2008**, *18*, 149–153.